DTIC
SELECTED
NOV 07 1995
F

19951103 034

Physical Evaluation
of the
Integrated Helmet and Display Sighting System
(IHADSS)
Helmet Display Unit (HDU)

By

Thomas H. Harding
Howard H. Beasley
John S. Martin

UES, Inc.

and

Clarence E. Rash

Aircrew Health and Performance Division
U.S. Army Aeromedical Research Laboratory
Fort Rucker, Alabama 36362-5292

August 14, 1995

Approved for public release; distribution unlimited.

DTIC QUALITY INSPECTED 1

U.S. Army Aeromedical Research Laboratory
Fort Rucker, Alabama 36362-0577

Notice

Qualified requesters
Qualified requesters may obtain copies from the Defense Technical Information Center (DTIC), Cameron Station, Alexandria, Virginia 22314. Orders will be expedited if placed through the librarian or other person designated to request documents from DTIC.

Change of address
Organizations receiving reports from the U.S. Army Aeromedical Research Laboratory on automatic mailing lists should confirm correct address when corresponding about laboratory reports.
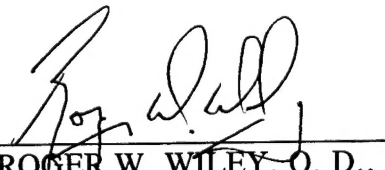
Disposition
Destroy this document when it is no longer needed. Do not return it to the originator.
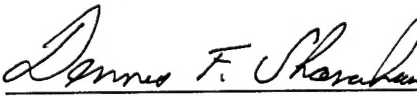
Disclaimer
The views, opinions, and/or findings contained in this report are those of the author(s) and should not be construed as an official Department of the Army position, policy, or decision, unless so designated by other official documentation. Citation of trade names in this report does not constitute an official Department of the Army endorsement or approval of the use of such commercial items.

Reviewed:

RICHARD R. LEVINE
LTC, MS
Director, Aircrew Health
 and Performance Division

Released for publication:

ROGER W. WILEY, O. D., Ph.D.
Chairman, Scientific
 Review Committee

DENNIS F. SHANAHAN
Colonel, MC, MFS
Commanding

REPORT DOCUMENTATION PAGE

Form Approved
OMB No. 0704-0188

1a. REPORT SECURITY CLASSIFICATION Unclassified		1b. RESTRICTIVE MARKINGS	
2a. SECURITY CLASIFICATION AUTHORITY		3. DISTRIBUTION/AVAILABILITY OF REPORT Approved for public release; distribution unlimited	
2b. DECLASSIFICATION/DOWNGRADING SCHEDULE			
4a. PERFORMING ORGANIZATION REPORT NUMBER(S) USAARL Report 95-32		5. MONITORING ORGANIZATION REPORT NUMBER(S)	
6a. NAME OF PERFORMING ORGANIZATION U.S. Army Aeromedical Research Laboratory	6b. OFFICE SYMBOL *(If applicable)* MCMR-UAS-VS	7a. NAME OF MONITORING ORGANIZATION U. S. Army Medical Research and Materiel Command	
6c. ADDRESS *(City, State, and ZIP Code)* P.O. Box 620577 Fort Rucker, AL 36362-0577		7b. ADDRESS *(City, State, and ZIP Code)* Fort Detrick Frederick, MD 27102-5012	
8a. NAME OF FUNDING/SPONSORING ORGANIZATION	8b. OFFICE SYMBOL *(If applicable)*	9. PROCUREMENT INSTRUMENTS IDENTIFICATION NUMBER	

8c. ADDRESS *(City, State, and ZIP Code)*	10. SOURCE OF FUNDING NUMBERS			
	PROGRAM ELEMENT NO. 0602787A	PROJECT NO. 787A879	TASK NO. PE	WORK UNIT ACCESSION NO. 164

11. TITLE (Include Security Classification)

(U) Physical Evaluation of the Integrated Helmet and Display Sighting System (IHADSS) Helmet Display Unit (HDU)

12. PERSONAL AUTHOR(S)
Thomas H. Harding, Howard H. Beasley, John S. Martin, Clarence E. Rash

13a. TYPE OF REPORT Final	13b. TIME COVERED FROM_____ TO _____	14. DATE OF REPORT *(Year, Month, Day)* 1995 August	15. PAGE COUNT

16. SUPPLEMENTARY NOTATION

17. COSATI CODES			18. SUBJECT TERMS *(Continue on reverse if necessary and identify by block number)*
FIELD	GROUP	SUB-GROUP	AH-64, helmet display unit, testing and evaluation, optical performance
23	02		
06	05		

19. ABSTRACT (Continue on reverse if necessary and identify by block number)

The Helmet Display Unit (HDU) of the Integrated Helmet and Display Sighting System (IHADSS) of the AH-64 Apache helicopter was evaluated to establish baseline data for performance figures-of-merit for comparison of future helmet mounted display designs. Measured parameters included physical and optical eye relief, exit pupil size, and position, field-of-view, luminance range, transmittance and reflectance characteristics, and static and temporal response.

20. DISTRIBUTION/AVAILABILITY OF ABSTRACT ☒ UNCLASSIFIED/UMLIMITED ☐ SAME AS RPT. ☐ DTIC USERS.	21. ABSTRACT SECURITY CLASSIFICATION Unclassified	
22a. NAME OF RESPONSIBLE INDIVIDUAL Chief, Science Support Center	22b. TELEPHONE *(Include Area Code)* (334) 255-6907	22c. OFFICE SYMBOL MCMR-UAX-SS

DD Form 1473, JUN 86   *Previous editions are obsolete.*   SECURITY CLASSIFICATION OF THIS PAGE

This page intentionally left blank.

Table of contents

List of figures

List of tables

This page intentionally left blank.

Introduction

The AH-64 Apache helicopter was fielded in June 1985. It is the U.S. Army's most modern attack aircraft. Integral to the AH-64 is the helmet-mounted display (HMD) system by which the pilot and copilot view pilotage and fire control imagery. This system is known as the Integrated Helmet and Display Sighting System (IHADSS). The IHADSS consists of various electronic components and a helmet/display system, called the Integrated Helmet Unit (IHU). The IHU includes a helmet, visor housings with visors, miniature cathode ray tube (CRT), and helmet display unit (HDU) [Figure 1]. The HDU serves as an optical relay device which conveys the image formed on the CRT through a series of lenses, off a beamsplitter (often called a combiner), and into the aviator's right eye (Figure 2). The CRT is one inch in diameter and uses a P-43 phosphor. The combiner is a multilayered dichroic filter which is maximized for reflectance at the peak emission of the P-43 phosphor.

The IHADSS operates in conjunction with two forward looking infrared (FLIR) sensors located on the nose of the aircraft. One sensor, called the Pilot's Night Vision System (PNVS), provides pilotage imagery while the second sensor, the Target Acquisition and Designation System (TADS), provides targeting imagery. [See Figure 3.] Infrared detectors, mounted on the IHU helmet, allow the FLIR sensors to be slaved to the pilot's head movements. Aircraft parameter symbology, along with the imagery from the FLIR sensor, is presented to the pilot by means of the HDU. The HDU is designed so that the image of the 30-degree vertical by 40-degree horizontal field-of-view (FOV) of the sensor subtends a 30- by 40-degree field at the pilot's eye. The IHADSS is a monocular display, presenting imagery to the right eye only. At night and under inclement weather conditions, the HDU imagery can be the sole source of information by which the pilot flys the aircraft. The visual quality of this imagery is of supreme importance.
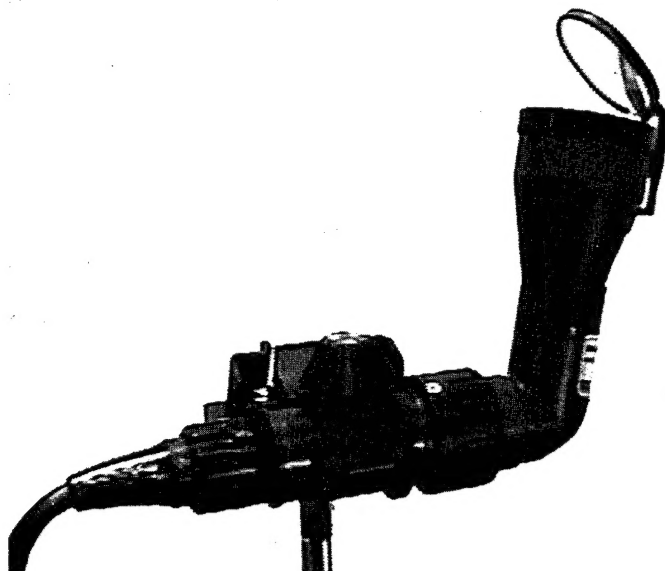

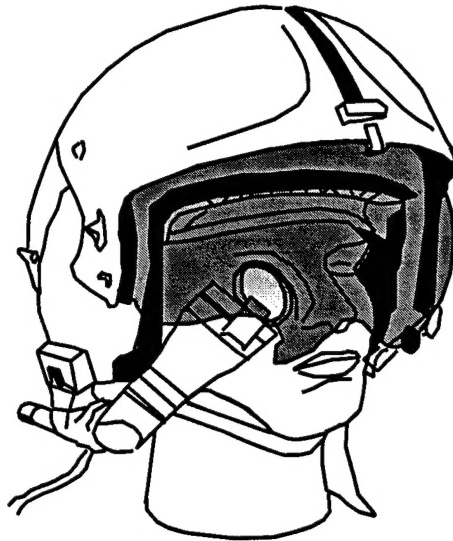
Figure 1. Helmet display unit (HDU)
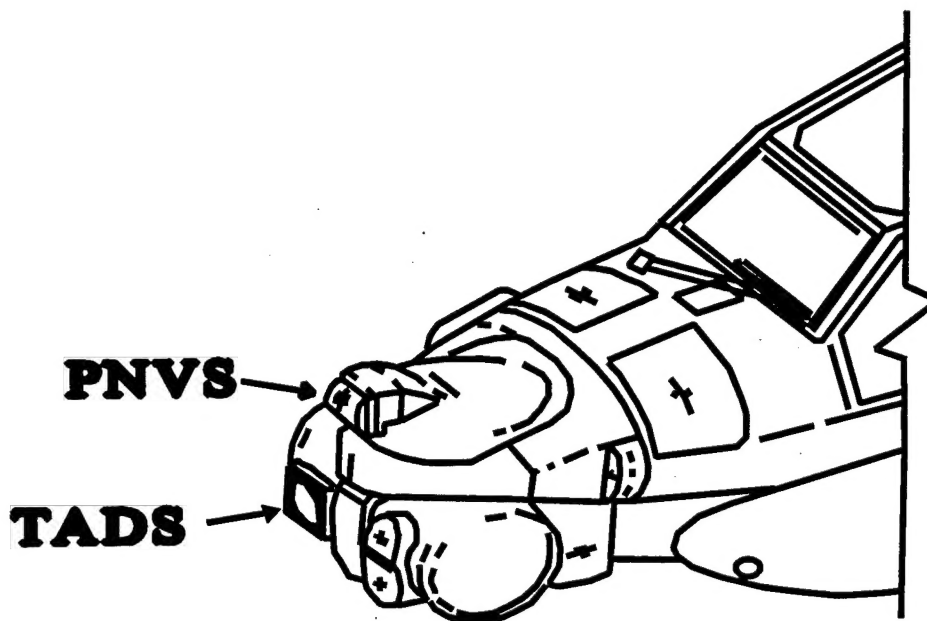
Figure 2. Aviator wearing HDU.

Figure 3. Nose of AH-64 helicopter with mounted thermal sensor (PNVS) and Target Acquisition Display System (TADS).

The U.S. Army has an ongoing program for the design and fielding of a modernized reconnaissance helicopter, the RAH-66 Comanche. An improved, biocular HMD design is planned for this aircraft. To ensure an improvement in HMD performance is achieved in the new generation display, an evaluation of the HDU performance was conducted. This evaluation will be used as a baseline for comparison of future display systems.

This paper reports the results of a battery of physical image quality figures-of-merit tests performed on imagery presented on a production (April 1992) IHADSS helmet display unit and cathode ray tube. The physical evaluation of the HDU imagery consisted of the optical tests listed in Table 1. This assessment encompassed the optical characteristics of the image generation subsystem and the relay optics. The image generation subsystem consisted of a miniature, 1-inch diameter, cathode ray tube display with field flattening lens. The relay optics consisted of the prism and lenses incorporated into the barrel of the HDU and the beamsplitter (combiner lens).

Table 1.

Physical measurements of the IHADSS HDU.

Exit pupil size	HDU spectral output
Eye relief (optical and physical)	Combiner lens
Field-of-view	Distortion
Luminance range	Spherical/astigmatic aberration
Contrast range	Temporal response
Grey levels	Spatiotemporal MTF

Exit pupil size, position and eye relief

In Figure 4, the IHADSS is shown in three configurations. In A, the HDU is shown without the combiner lens in place, while in B, the HDU combiner lens is fully retracted, and in C, the HDU combiner lens is fully extended. These three configurations constitute the three test conditions in which we made the measurements noted in the figure. Each distance measurement was made independently of any other measurement. The exit pupil diameter, P, was measured under the three conditions as was the optical distance from the objective lens to the exit pupil. In configurations B and C physical eye relief, R, also was measured. From these three configurations, certain arithmetic equalities emerge and form a basis for assessing measurement

accuracy. These identities are

$$P_1 = P_2 = P_3 \qquad (1)$$

$$A_1 + C_1 = A_2 + C_2 = A_3 \qquad (2)$$

$$C_1 = C_2 - E \qquad (3)$$

where A equals the distance from the exit pupil to the center of the combiner and E equals the total amount of extension available for the combiner

For these measurements the CRT was replaced with a Honeywell, Inc. CRT simulator* (P/N/ 1C1C6981-1C1), which was effectively a specially designed flashlight. The CRT simulator was designed to conform to the HDU barrel and was fitted with a field flattening lens. The CRT simulator has a test target on it that clearly shows the center of the field with crossed lines. This center target is used to optically align the HDU with a measuring telescope. The HDU has a focus adjustment which allows a minimum range of ± 3 diopters. The CRT simulator did not incorporate a focus adjustment. Therefore, a diopterscope was used to confirm a minus 1 diopter setting, which was achieved using an O-ring. The selection of a minus 1 diopter setting was somewhat arbitrary, but was representative of typical pilot settings.

Configuration A: No combiner lens

Exit pupil size. The exit pupil of the HDU was expected, by ray tracing, to be circular in shape. This would allow its size to be defined by its diameter. To measure the size of the exit pupil, we positioned the HDU, without the combiner lens in place, such that the exit pupil formed would be centered over an optical bench and optically aligned with a telescope mounted to the optical bench (Figure 5). Optical alignment was achieved by positioning the HDU until the center of the test target was aligned with the telescope which was aligned previously to the center of the optical bench. The telescope was focused on the circular exit pupil. When viewed through the telescope, a circular disk of light was seen in sharp focus. The telescope was equipped with accurate vertical and horizontal computer driven stepping motors with 0.1 micron incremental precision. The telescope's eyepiece had a cross hair reticle with extended vertical and horizontal lines. An observer positioned the vertical cross hair on one side of the circular patch of light such that the cross hair was just tangent to the circle's outer border. The position on the stepping motor controller was set to zero and the cross hair moved to the opposite side of the patch. On this side the cross hair was positioned just on the inside edge of the light border. In this fashion, the thickness of the cross hair would not influence our results. The distance traveled by the telescope (i.e., exit pupil diameter) then could be read from the stepping motor controller. Four additional measurements of the horizontal diameter were taken, then the procedure was repeated for the vertical diameter. The horizontal diameter measured 10.577 $\pm$ 0.023 mm. (Note: All error measurements are $\pm$ 1 standard deviation.)
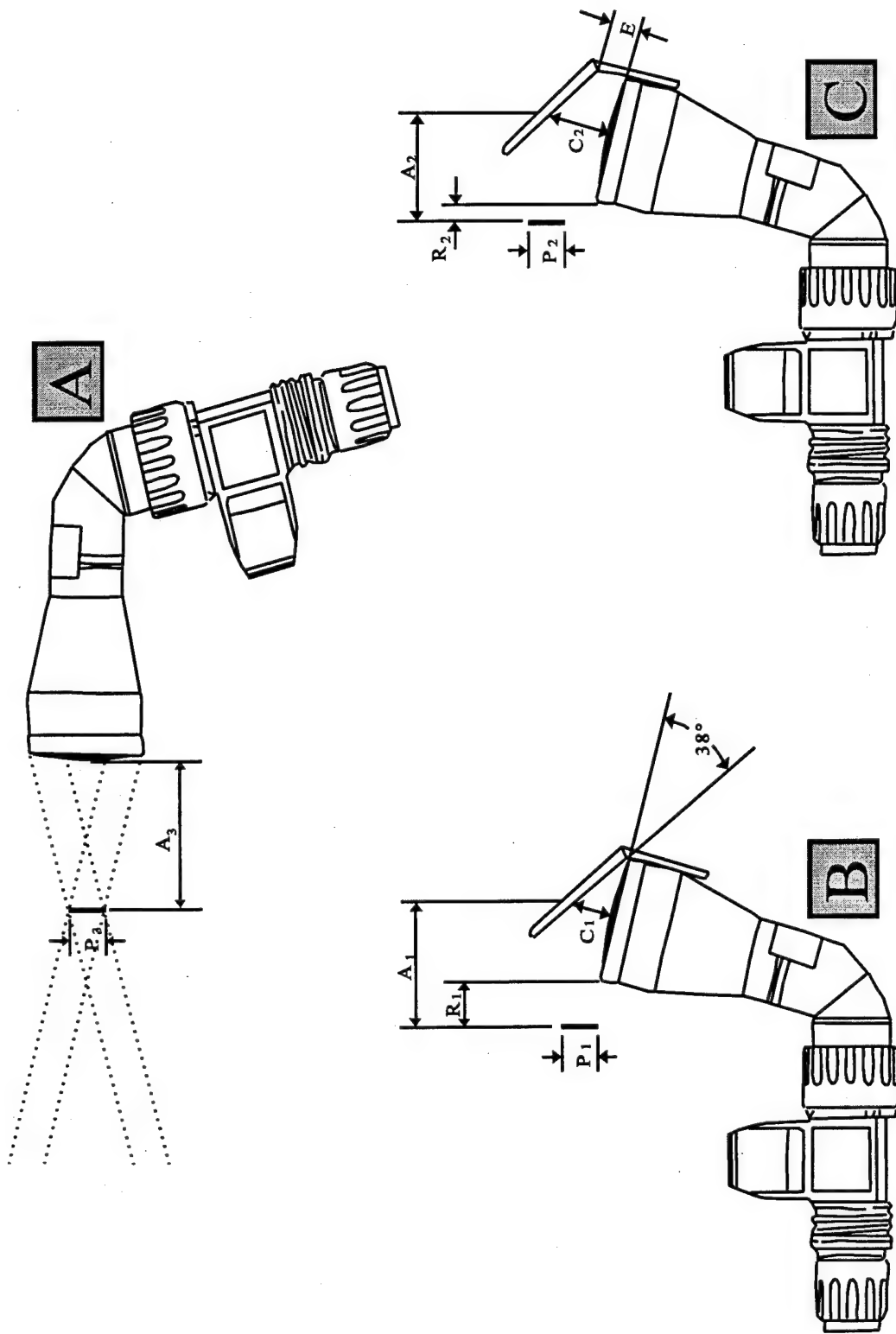
---

* See Appendix.

Figure 4. Schematic of physical measurement configurations of the HDU.
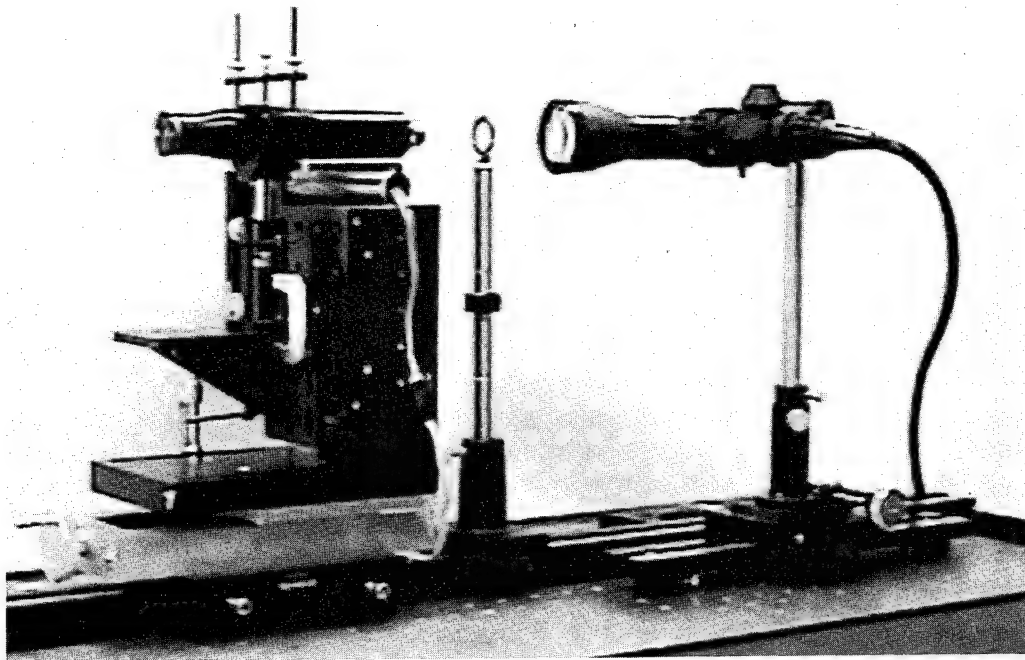
Figure 5. HDU (without the combiner lens in place) test setup for measurement of exit pupil size, position, and eye relief.

and the vertical diameter measured 10.53 5 ± 0.011 mm. Since the measurements were so close, we combined the measures to provide our estimate of exit pupil diameter ($P_3 = 10.556 \pm 0.028$ mm). The vertical diameter measured 10.535 ± 0.011 mm. Photographic documentation of the exit pupil's circular shape is provided in Figure 6.

Exit pupil position. To measure the distance between the exit pupil and the last lens element, the objective lens, in the HDU barrel requires knowledge of the exit pupil's position in space. We developed an observer method for locating the position of the exit pupil and measuring its distance to the HDU objective lens. We aligned the HDU with the measuring telescope as above and located the approximate position of the exit pupil by moving a rear projection screen along the optical bench until we noted the exit pupil's smallest diameter imaged on the screen. Fixing the rear projection screen at this position with a linear micrometer, we focused the telescope on the image formed on the screen. The diameter of the imaged exit pupil was measured as above. The measurements were repeated until we had five independent measures of the horizontal diameter. The rear projection screen then was systematically moved fore and aft along the optical axis and the procedure repeated. During this procedure, the observer received no feedback on his performance. A graph of our results is shown in Figure 7.

Figure 6. Photograph of exit pupil.

Note the 'V' shaped curve with the apex marking the position of the exit pupil. At the apex, the horizontal diameter of the exit pupil measu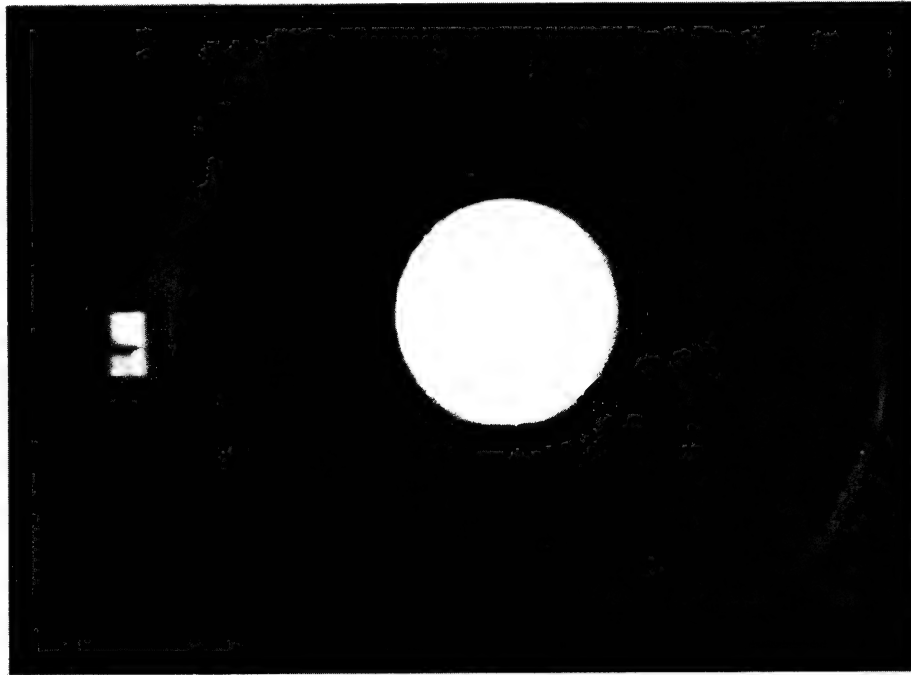red 10.586 ± 0.030 mm, which was extremely close to the 10.577 mm measured without the rear projection screen. The brackets at each data point represent one standard deviation above and below the mean of the five observations. The method yielded a highly reliable method of locating the spatial position of the exit pupil. Placing the rear projection screen at the location corresponding to the smallest exit pupil diameter, we measured the distance from the surface of the HDU objective lens to the rear projection screen (measurement A_3). The rear projection screen was held in place by circular rings which clamped the screen between them. When viewed from the side, the thin material appeared sandwiched between the circular rings and made a highly visible and accurate target for the exit pupil position. A parallel optical bench was placed close to the one supporting the rear projection screen and telescope. A second short working distance telescope was placed on a slide positioner and the telescope aligned such that an observer could telescopically view the edge of the rear projection screen and place the vertical cross hair over it. Noting this position on the positioner, the telescope was moved, and the vertical cross hair was aligned with the side of the rear surface of the HDU's objective lens. Marking this position, we could calculate the distance traveled by the telescope and, hence, the distance from the last lens element to the exit pupil. We repeated these measurements four times, thus providing five independent measures of distance A_3. We found a mean distance of 57.66 mm with a standard deviation of ± 0.049 mm. This distance is defined as the optical eye relief.

11
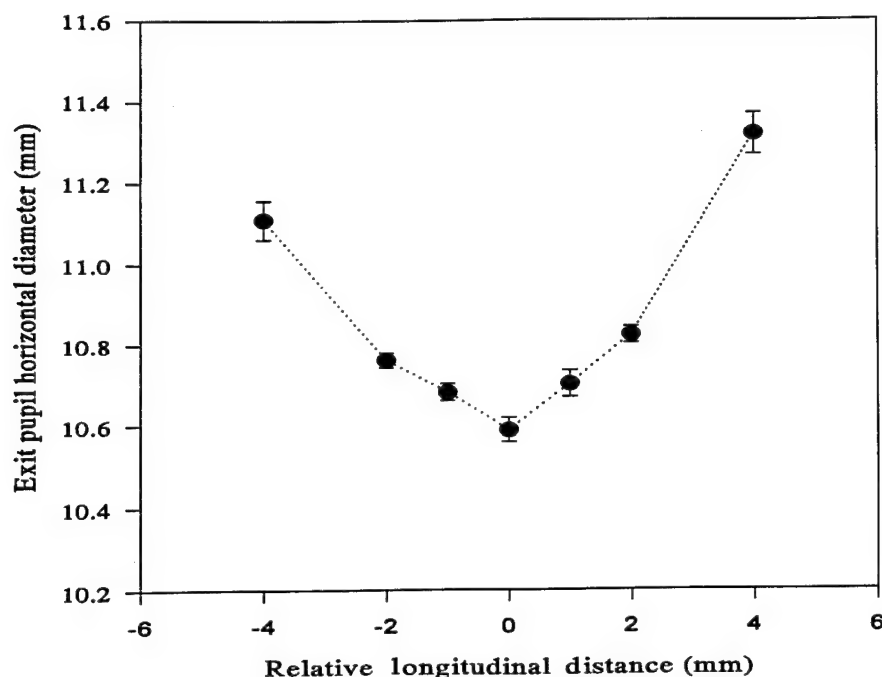
Figure 7. Behavioral assessment of exit pupil longitudinal position.
Position 0 marks the position of the exit pupil. The error bars
are ± 1 standard deviation.

Configuration B: Combiner lens retracted

Exit pupil size and position. The apparatus and test setup for the measurements depicted in configuration B are presented in Figure 8. As above, the optical telescope was mounted to the precision x-y positioning system which was in turn mounted to the optical rail, and the rear projection screen was mounted to the same optical rail via a translation rod carrier with 0.1 mm resolution. The combiner lens was mounted on the HDU and was retracted fully. The main barrel of the HDU was mounted along side the optical rail such that the combiner lens essentially was centered over the optical rail. In this position, the CRT simulator test target was aligned with the telescope cross hair. In practice, this alignment was achieved only after considerable adjustments were made to the position of the HDU. This alignment was best performed when the HDU's barrel was placed parallel to the optical axis of the telescope and screen.

The size of the exit pupil was measured using the same technique as described above by focusing on the exit pupil formed in space and meauring its horizontal and vertical diameter. Again, five independent measures of each diameter were made. The vertical diameter equaled 10.626 ± 0.022 mm and the horizontal diameter equaled 10.548 ± 0.025 mm. Averaging yielded the exit pupil diameter ($P_1 = 10.587 \pm 0.0451$ mm).

12

Figure 8. HDU (with the combiner lens) test setup for measurement of exit pupil size, position, and eye relief.

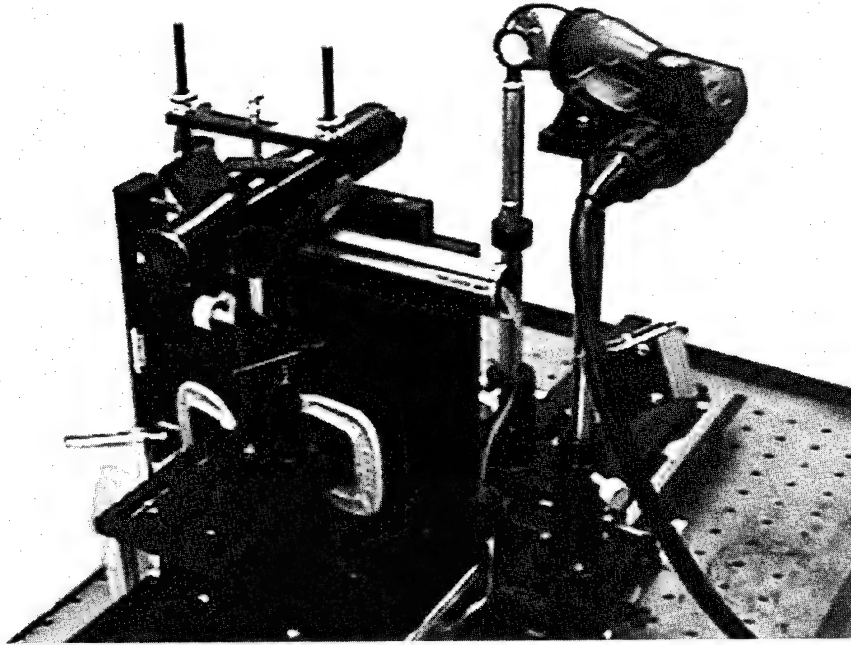*Eye relief.* The optical eye relief of an optical system is defined as the distance along the optical axis from the last optical element to the exit pupil (measurement A_1 in Figure 4). While an important parameter to an optical designer, the optical eye relief value often is misleading. Of greater importance in helmet-mounted displays is the minimum clearance from the closest display system component to the eye or exit pupil (measurement R_1 in Figure 4). Referred to as physical eye relief or eye clearance distance, this parameter determines system compatibility with auxiliary devices, e.g., corrective lenses, protective masks, etc.

The design specification for optical eye relief for the IHADSS* (Hughes Helicopters, Inc., 1982) was that the eye relief would be at least 10 millimeters (mm) as measured from the center of the combiner lens.

To measure eye relief, we first located the position of the exit pupil using the rear projection screen. Using the same technique as before, we located the position of the exit pupil to the nearest 0.5 mm. Knowing the position of the exit pupil, we measured the distance from the middle of the combiner lens to the exit pupil. The middle of the combiner lens was found by viewing the test target from a position normal to the objective lens. Focusing a telescope to infinity, we positioned the telescope such that the cross hairs and the test target center aligned properly. Focusing the telescope on the combiner lens, a marker was placed on the combiner lens at the position of the telescope's cross hair, thus marking the middle of the combiner lens. Mounting a parallel rail on the side opposite the HDU, a short working distance telescope was mounted to the parallel rail via a slide positioner and positioned to measure distances A_1 and R_1.

13

As in our measurement of distance A_3, five independent measurements were made for each distance. We found a mean optical eye relief, A_1, of 40.12 ± 0.04 mm and a mean physical eye relief, R_1, of 13.18 ± 0.04 mm. The distance C_1, the distance from the middle of the objective lens to the middle of the combiner lens, was measured with a micrometer. This distance measured 16.12 mm.

Condition C: Combiner lens fully extended

    Exit pupil size and position, and eye relief. Using the same test setup in Figure 8, with the exception that the combiner was fully extended, we made the measurements depicted in configuration C as presented in Figure 4. Following optical alignment of the fully extended combiner lens, the exit pupil was measured as before with a telescope mounted to a precision positioner. Following five independent measures, we found the vertical diameter equaled 10.591 ± 0.011 mm and the horizontal diameter equaled 10.502 ± 0.010 mm. Averaging yielded the exit pupil diameter ($P_2 = 10.546 \pm 0.046$ mm). Using the rear projection screen, the position of the exit pupil was found using the pupil diameter measurement technique. The position of the telescope was moved in 0.5 mm increments. Positioning the rear projection screen at the exit pupil, the optical and physical eye relief distances (A_2 and R_2, respectively) were measured with a second telescope. Again five independent measures were made and the results were $A_2 = 25.76 \pm 0.049$ mm, and $R_2 = -5.988 \pm 0.010$ mm. The negative value found for R_2 means that there was a negative physical eye relief. The exit pupil was within the lateral line marked by the edge of the HDU housing at the objective lens.

    The distance between the combiner lens and the objective lens, C_2, was measured with a micrometer and was found to be 32.67 mm. Also with a micrometer, the combiner extension (E) could be measured with a micrometer, and this distance was found to be 16.40 mm.

Consistency and accuracy of measurements

    From equation 1, we know that P_1, P_2, and P_3 should be identical since a reflection from the combiner lens should not affect exit pupil diameter. From Table 2, we see that our measures have an average spread of 0.041 mm. This spread represents a 0.39 percent variation given a mean exit pupil diameter of 10.573 mm. From equation 2, we find that

$$A_1 + C_1 = A_2 + C_2 = A_3.$$

Substituting values from Table 2, we find a spread of 2.19 mm. This spread represents a 3.81 percent variation given a mean value of 57.44 mm. This percent variation seems high, although it should be expected when considering the difficulty of locating the exact center of the combiner lens and finding the position of the exit pupil. The position of the exit pupil, was measured to the nearest 0.5 mm for P_1 and P_2 and to the nearest 1 mm for P_3.

    Equation 3 relates to the combiner extension and its effect upon physical eye relief. Substituting values from Table 2 for equation 3, we find a 0.15 mm error which represents a 0.93

percent variation from the mean of 16.195 mm. As can be seen, our measurements were free of significant error and, therefore, our measurement technique seems reliable and provides a high degree of accuracy.

Field-of-view (FOV)

Field-of-view was measured by rotating the HDU about a point that was fixed at the center of the exit pupil. By ray tracing, it can be demonstrated that the image displayed by the HDU is contained within a cone whose apex is at the exit pupil and extends out into space. By measuring luminance within this cone, we could measure the extent of the formed image. We displayed a test pattern on the HDU's miniature CRT which clearly marked the center of the CRT. By aligning a photometer with the exit pupil and with the center of this test pattern, we were able to view the test pattern as the system was rotated about the exit pupil. After this alignment was achieved, we replaced the test pattern with a uniform luminance which covered the full extent of the CRT. Adjusting the photometer to focus at the exit pupil, we could measure the luminance at the exit pupil as the HDU was rotated and thus measure the field-of-view. Figure 9 shows a plot of the luminance data. The data were relatively flat with a precipitous fall-off at the edges of the field-of-view. The horizontal field-of-view measured approximately 40 degrees and the vertical field-of-view measured approximately 31 degrees.

Luminance range and contrast ratios

The luminance range of the miniature CRTs is quite extensive although it is limited by spectral filtering, the HDU amplification circuits and the typical operational/user settings. By focusing at the exit pupil formed by the HDU, we found a maximum luminance output of 640 fL at saturation. We measured the CRT luminance loss through the HDU to be about 46 percent which is due mainly to the elimination of the side lobes in the P-43 phosphor spectrum (Fig. 10a and b). Thus the output of the CRT at saturation is about 1200 fL. We drove the CRT with an NTSC video signal where the luminance profile was a bright bar set to maximum and its leading and trailing edges set to minimum. We measured contrast ratios by focusing a photometer through the exit pupil to the center of the HDU's field-of-view (focus set to near infinity), and then the contrast was reversed and the luminance measurement repeated.

By adjusting the brightness and contrast potentiometers in the HDU amplifier to maximum, we found a contrast ratio at saturation to be about 3.0 (640/210). To define the contrast ratio over a more usable operational range, we made measurements at two peak luminance levels. The two levels we chose were 15 fL and 150 fL to correspond with lighting conditions encountered while flying with ANVIS and under day time conditions. Operational directions on the use of the HDU indicates that brightness should be adjusted until it is just seen and then contrast adjusted to obtain differentiation between the shades of gray in a test target.

Table 2.

Distance measures from Figure 4.

Measurement	Distance	Standard deviation
P_1	10.587 mm	0.045 mm
P_2	10.546 mm	0.046 mm
P_3	10.586 mm	0.030 mm
A_1	40.120 mm	0.040 mm
A_2	25.76 mm	0.049 mm
A_3	57.66 mm	0.049 mm
R1	13.18 mm	0.040 mm
R2	-5.988 mm	0.010 mm
C1	16.12 mm	N.A.
C2	32.67 mm	N.A.
E	16.40 mm	N.A.

With this guidance in mind, we took the following approach: with the contrast set to zero, we adjusted the peak brightness to 1 fL, measured at the target bar's peak. We then adjusted contrast until we achieved a luminance of either 15 fL or 150 fL at the peak. Under these conditions, we found contrast ratios of 13.6 (15/1.1) and 33.3 (150/4.5).

Grey levels

If we define grey levels as being discrete and one-half octave apart, then the number of gray levels can be calculated from the contrast ratios specified above. For contrast ratios of 13.6 and 33.3, we find 8 and 11 gray levels, respectively. Over the luminance range of the IHADSS, different numbers of gray levels are available. However, these two ranges offer some of the largest gray scale ranges.
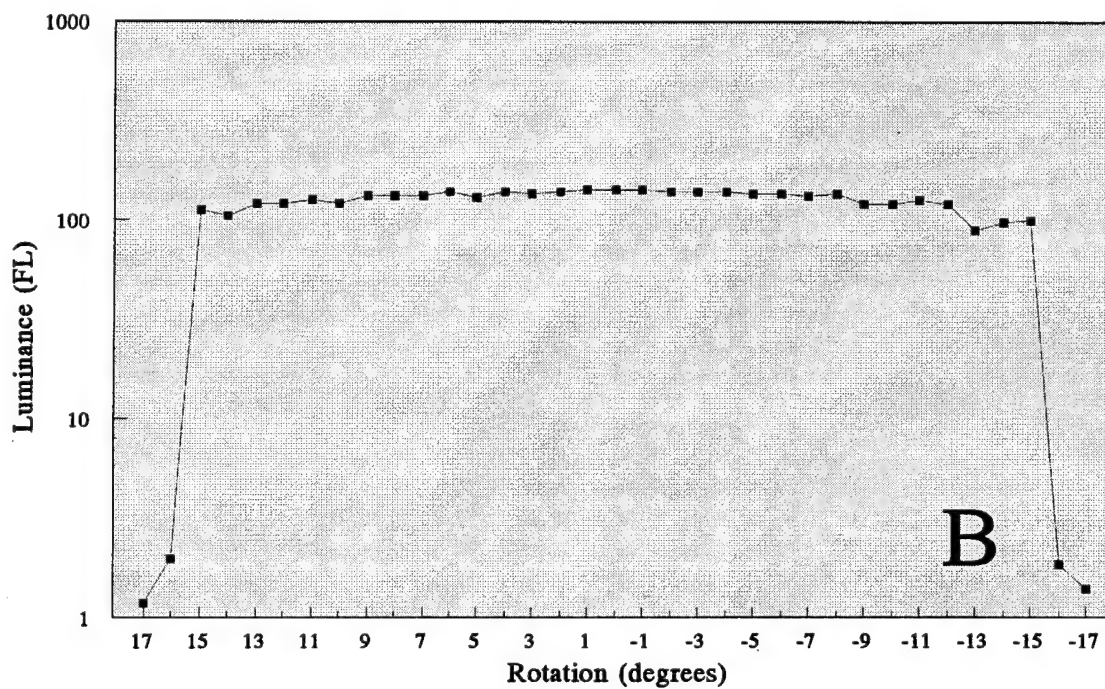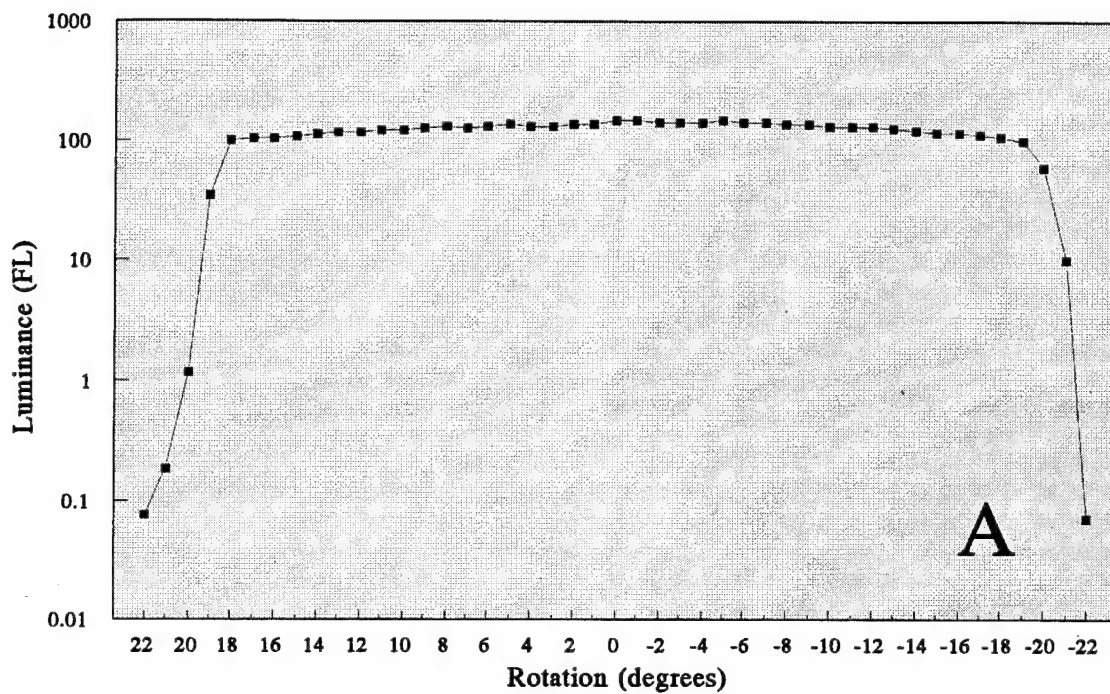
Figure 9. Luminance measurements showing the horizontal and vertical fields-of-view.
A - horizontal FOV, B - Vertical FOV.

Spectral output

The spectral output of the HDU was measured using a Photo Research's SpectraScan 704™* spectrophotometer and their SpectraView™* software. The spectral output of the HDU with the P-43 phosphor is narrow banded with a peak transmissivity at 544 nm (Figure 10). This peak corresponds with the peak of the P-43 phosphor. The width of the spectrum is about 4 to 6 nm at a level equal to 50 percent of the peak.

Combiner spectral transmittance and reflectance

The spectral transmittance of the combiner lens was measured using a EG&G Gamma Scientific RS-10A irradiance head as our light source. Its spectral output had sufficient power at each visible wavelength for reliable transmittance measurement. We used the SpectraScan 704 to measure the spectrum of the light source with and without the HDU combiner lens in the optical path. The filtered spectra was divided by the unfiltered source spectra, thus providing a transmittance curve for the combiner lens. Since the combiner lens is at an angle to the eye, we measured transmittance over a range of angular orientations. We estimate that the plane of the combiner lens is approximately 23 degrees off parallel to the front surface of the cornea. We took data from 0 to 40 degrees in 2-degree increments. Figure 11 shows the transmittance function at 22 degrees.

Assuming reflectance is equal to the light that is not transmitted through the combiner (assuming no absorption), then spectral reflectance is calculated by the following equation.

Reflectance = 1 - Transmittance

Reflectances were calculated from 0 degrees to 40 degrees. The combiner lens is coated to allow reflectance around the peak of the HDU output (544 nm with P-43 and P-53 phosphors). This peak reflectance we found to be sensitive to angular orientation. Figure 12 shows a graph of peak reflectances as a function of orientation. Note the peak shift to lower wavelengths with increasing angle. Since we measured the plane of the combiner lens to be 38 degrees off of the objective lens parallel plane (Figure 4), the data collected at that angle are most relevant. Figure 13 shows calculated reflectance at 38 degrees. The reflectance is relatively narrow band.
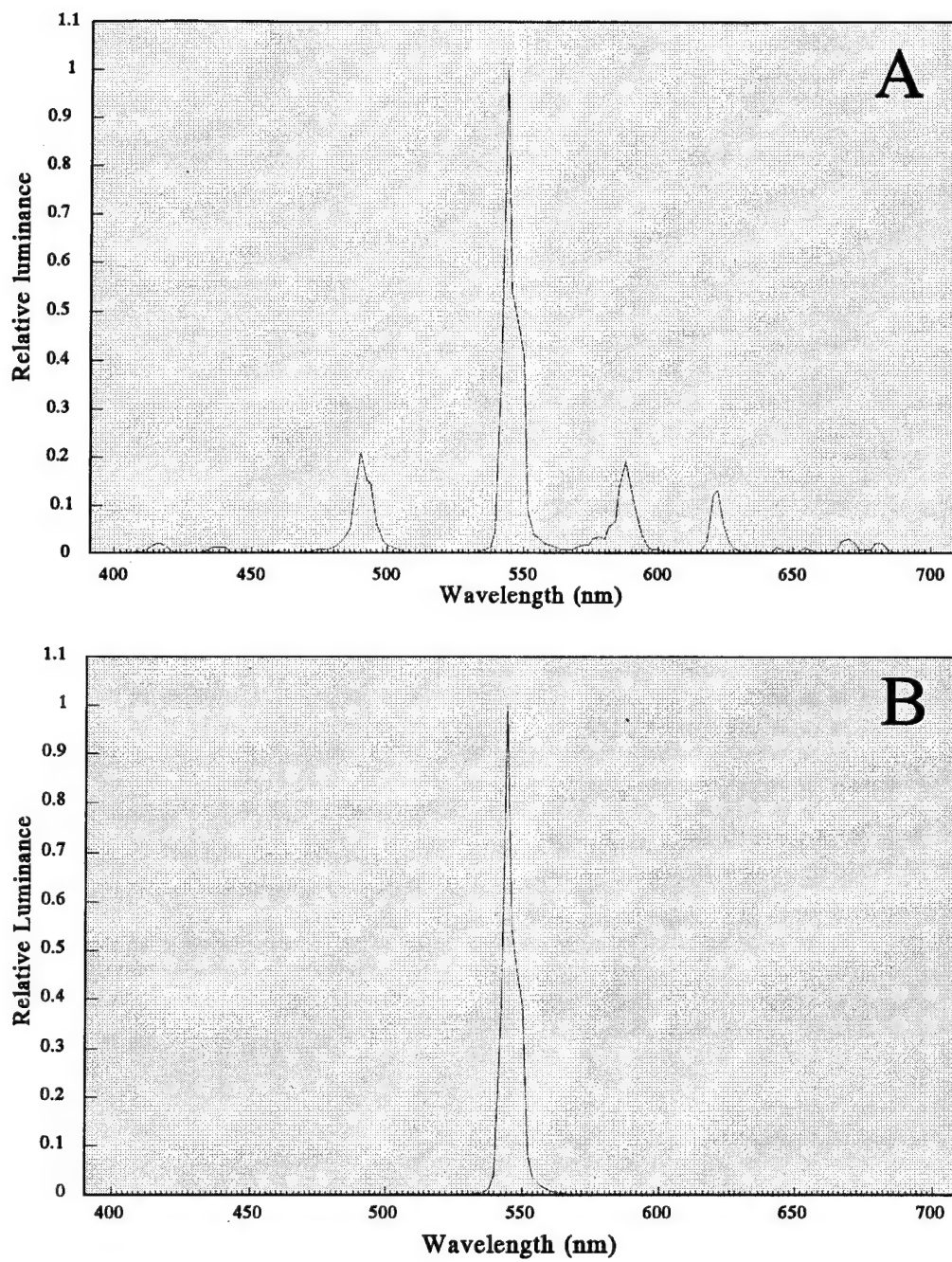
Figure 10. Spectra of a P-43 phosphor (A) and spectral output of the IHADSS
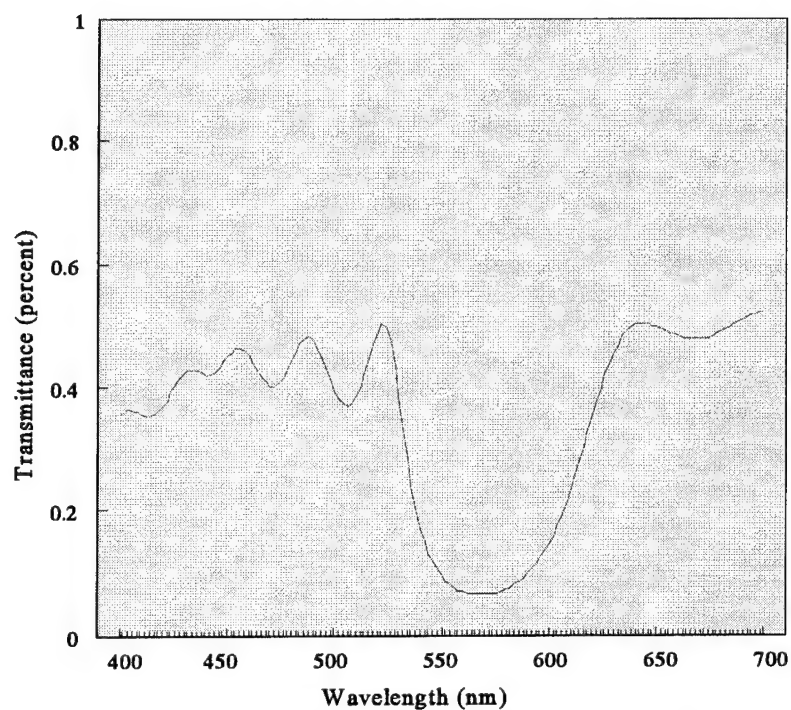HDU using a miniature P-43 phosphor (B).

Figure 11. Combiner lens transmittance measured with the
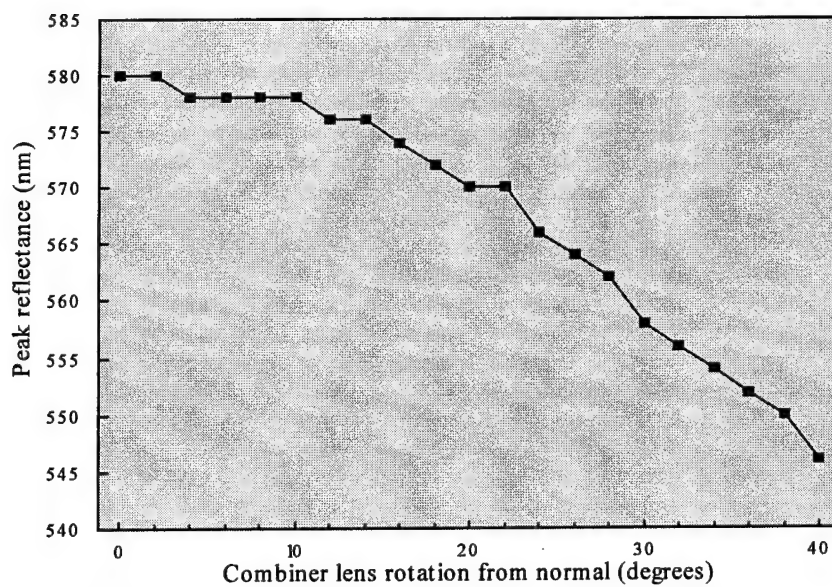combiner lens 22 degrees off normal.

Figure 12. Combiner lens peak reflectance as a function of
angular orientation.

Also plotted in Figure 13 is the spectral output of the HDU with a P-43 phosphor. The reflectance and output spectra provide a good compromise, allowing sufficient HDU luminance available to the aviator, while the broadband combiner transmittance spectra allows for adequate outside luminance to reach the aviator's eye.
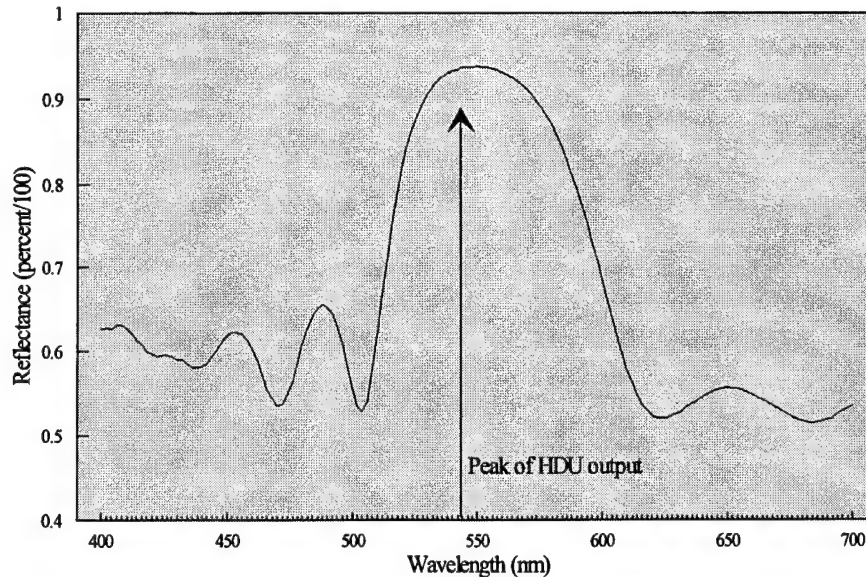

Figure 13. Combiner lens reflectance at 38 degrees off normal. Arrow marks the peak of the HDU output using a P-43 phosphor.

Distortion

Distortion was measured using a Ann Arbor optical tester*. The tester projected an image of a Ronchi ruling that passed through the combiner lens twice (Figure 14). The illuminated Ronchi ruling was positioned at the focal length of the lens which essentially collimated the light from the ruling. Moving the lens closer to the ruling increases the number of imaged lines. The light passed through the combiner, was reflected off the mirror, and passed through the combiner a second time. An image of the reflected ruling could be viewed or photographed through a lens atop the ruling. A photograph of the resulting image is shown in Figure 15. Distortion would show up as a warping or shear to the grating pattern, and, as seen in Figure 15, the ruling was clear with no apparent distortion. We examined distortion for different combiner angles, and no apparent distortion was observed.

Spherical/astigmatic aberration and field curvature

We measured field curvature using a dioptometer. As in the field-of-view measurements, the HDU was mounted to a rotating stage with the center of axis roughly equivalent to the position of the exit pupil. The dioptometer was mounted to the optical table and aligned with the
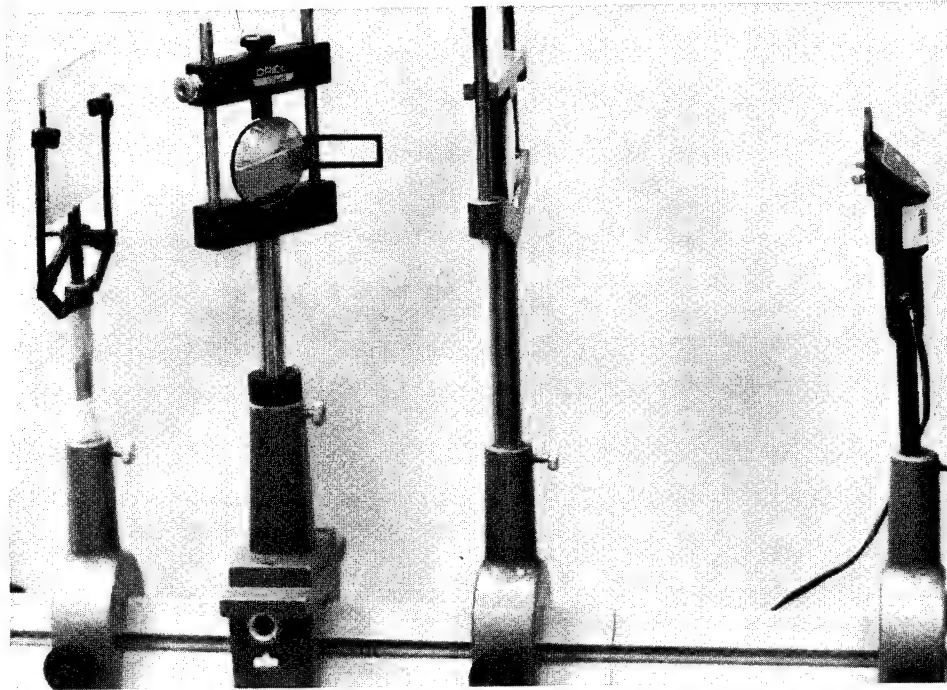
21

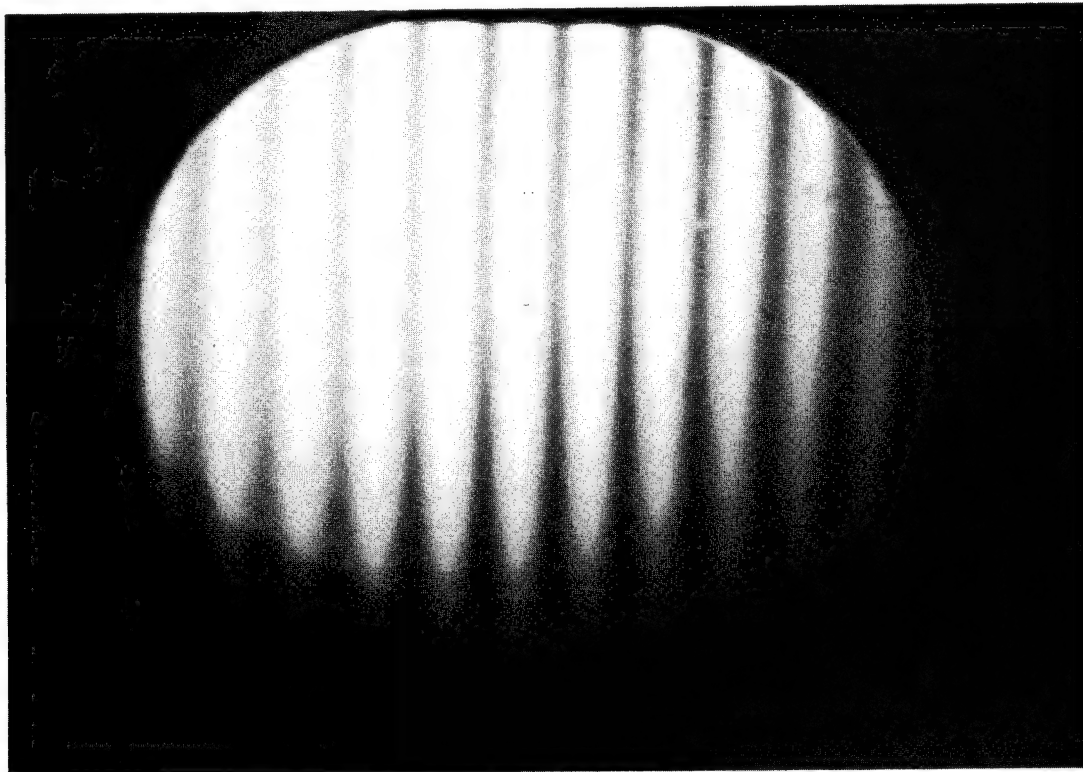Figure 14. Photograph of test setup for measuring optical distortion.

Figure 15. Image of Ronchi ruling after having passed through the combiner lens twice.

center of the test target (see Figure 16 for photograph of experimental test setup). The position of the exit pupil was formed at the front of the dioptometer. We adjusted the focus adjustment on the HDU until we had about a 0 diopter reading in the center of the display. During this adjustment, we took the opportunity to measure the focus range of the HDU using the dioptometer. We required auxiliary lenses to compensate for the limited two-diopter range of the dioptometer. The range of focus measured -6.25 to +3.625 diopters. Following alignment and focus adjustment, a grid of vertical and horizontal lines was displayed on the phosphor. Within each square formed by the intersecting vertical and horizontal lines, a small spot was displayed. During the course of our measurements, we noted while focusing on the lines that the spot would elongate in one direction and then the other as we went in and out of focus. This change in shape indicates an astigmatic error with the elongation of blur indicating the astigmatic axis. The axis was about 15 degrees off vertical at the 105 degree position. Therefore, we measured field curvature in the horizontal axis by focusing on the small spots. By rotating the HDU, we were able to traverse across the horizontal axis of the system. From -18 to +18 degrees, in one-degree increments, we measured field curvature by focusing on the small spots (Figure 17). Field curvature is shown as a change in diopter readings as a function of degrees of rotation. Field curvature ranged from -0.5 to 1.125 diopters.
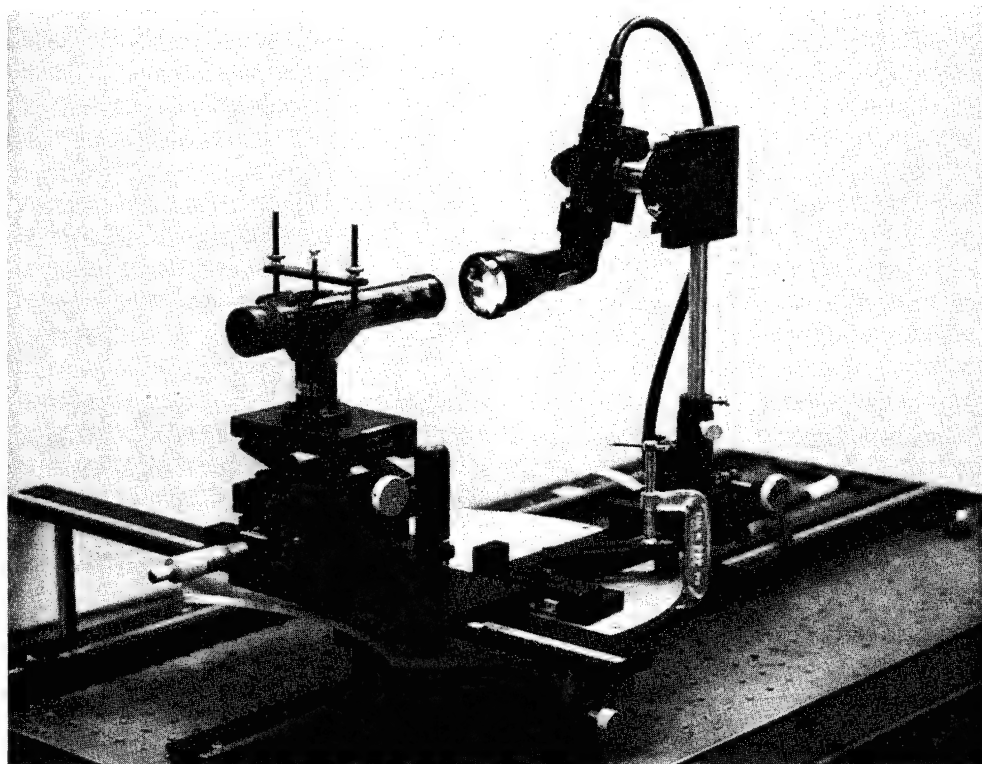

Figure 16. Photograph of experimental setup for measuring optical aberration.

Astigmatic error was measured by rotating the grid lines to coincide with the astigmatic axis. As we traversed the horizontal axis, we focused on the 105 degree lines and then the 15 degree lines. Astigmatic aberration is the difference between the diopter readings for the two foci. We plotted the difference between the two foci in Figure 17. Note that astigmatic error exceeded 1.5 diopters in the periphery.

Spherical aberration was measured using a dioptometer mounted to a precision traversing stage. The dioptometer was aligned with the center of the test target and then the test target was replaced with a grid of vertical and horizontal lines. Dioptometer readings were made at the center by focusing on the horizontal lines and then the vertical lines. Traversing the dioptometer laterally in 1-mm increments to each side, these measurements were repeated. Spherical aberration is seen as a change in focus over the lateral positions as shown in Figure 18. As above, astigmatic aberration is the difference between the horizontal and vertical diopter readings at each lateral position from center. Data are averaged from either side of center for lateral decentration to 5 mm. At 5 mm decentration, spherical aberration was still below 0.5 diopters. On one side of center, we were able to make a measurement at 6 mm. Since the exit pupil was approximately 10.5 mm, a decentration of 6 mm would be taking a reading at the edge of the pupil. Nevertheless, we plotted these points since our readings were repeatable.
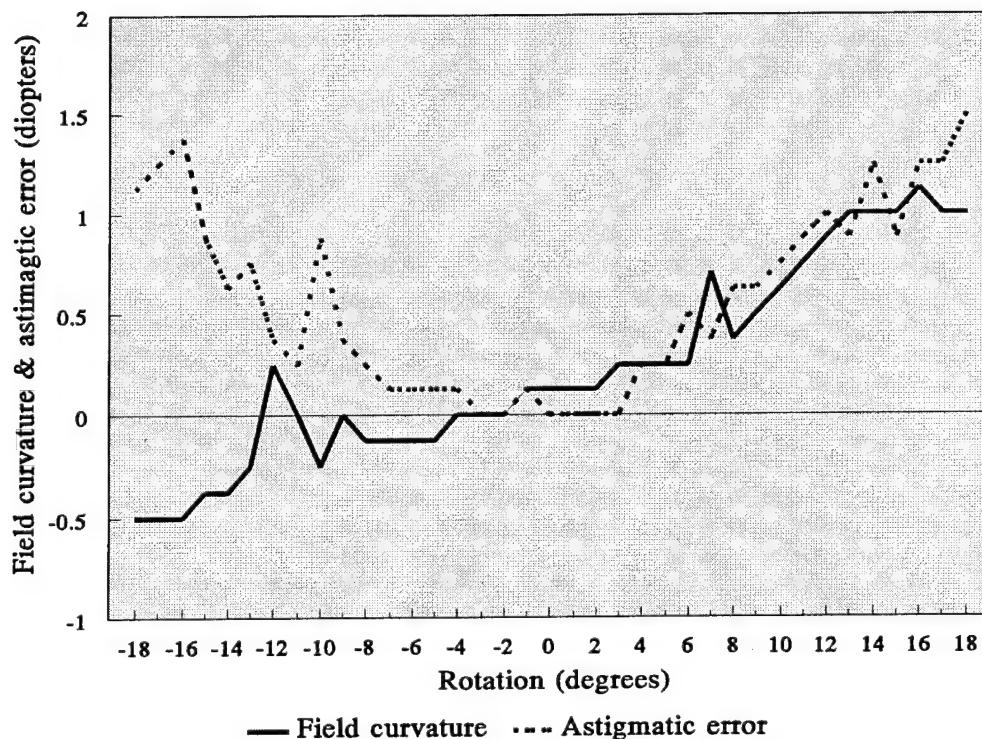

Figure 17. Field curvature and astigmatic aberration revealed as a function of degrees of angular rotation.
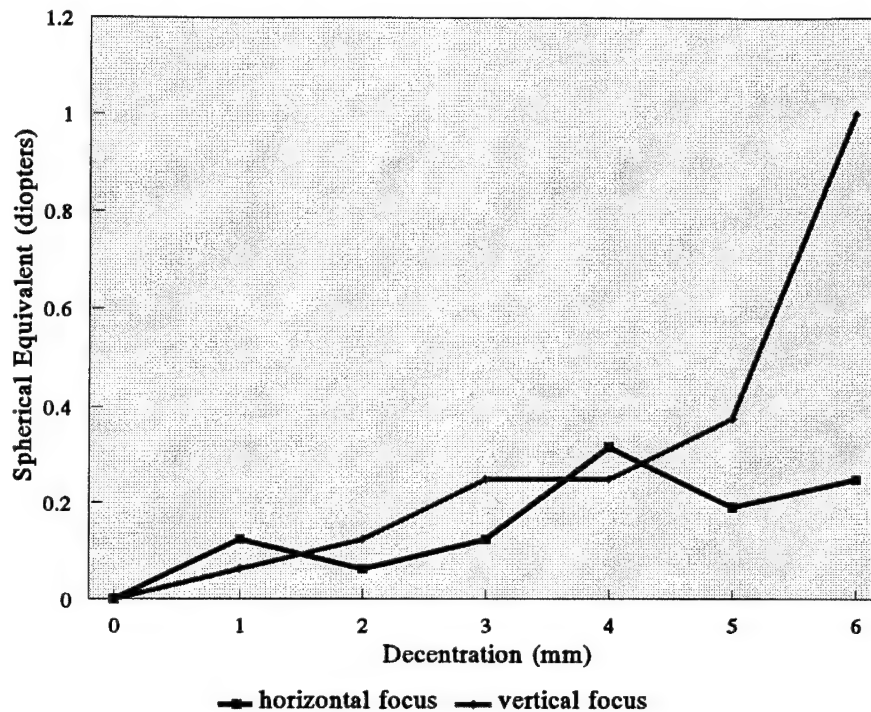
Figure 18. Spherical and astigmatic aberration as a function of
decentration. Data at 6 mm may be suspect with respect
to the size of the exit pupil.

Temporal response

The temporal response of the system was measured by sinusoidally modulating a spot at multiple temporal frequencies and measuring the luminance response. The peak and trough luminance responses were used to compute Michaelson contrast, $[(L_{max} - L_{min})/(L_{max} + L_{min})]$, where L is luminance. The test spots were square test targets of increasing size (from approximately 0.2 to 1 degree square). The test targets were located in the center of the display, and their luminance was measured using a Pritchard 1980A photometer*. An analog voltage signal from the photometer, whose voltage output was proportional to luminance, was fed ultimately into a Tektronix 2440* storage oscilloscope. In order to achieve a clean signal, the voltage signal from the photometer was first lowpass filtered to eliminate unwanted noise.   We used two active filters with a 30-Hz cutoff frequency. The highest temporal frequency tested was 16 Hz. The peaks and troughs of the sinusoidal voltage patterns were measured, and contrast values were calculated. All of the curves had the same shape and overlapped nicely when normalized. Figure 19 shows the averaged temporal frequency curve. Unexpectedly, the curve showed no tendency for fall-off and stayed flat out to 16 Hz.

25

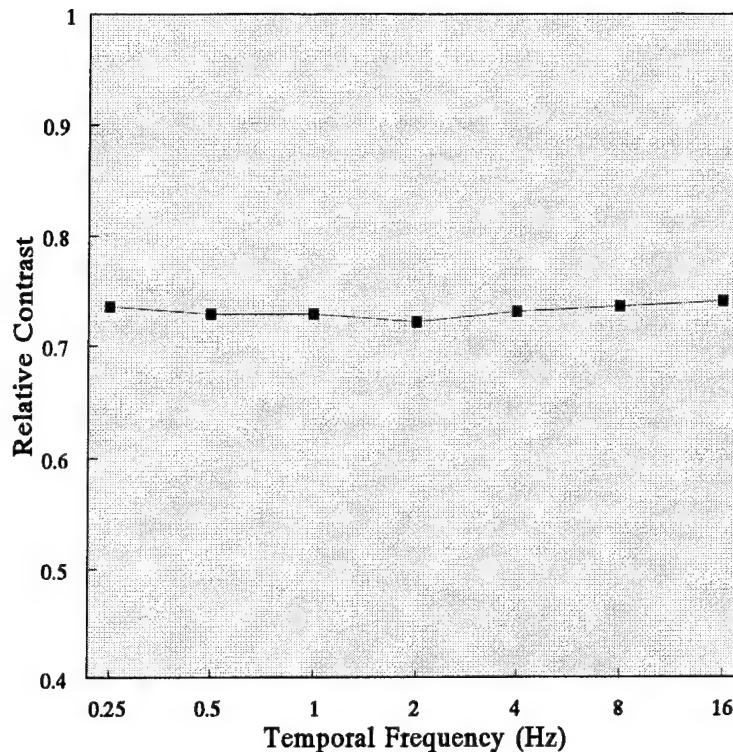Figure 19. Temporal response of the IHADSS HDU.

Spatiotemporal modulation transfer functions (MTFs)

The spatiotemporal MTF of the HDU was measured using drifting sinusoidal gratings. The gratings were generated by a Vision Research Graphics VisionWorks stimulus generator*. The output from the VisionWorks system was modified to produce a standard VGA signal. Modification was made to the Texas Instruments graphics accelerator (TIGA)* software drivers and to the VisionWorks software to accommodate the lower resolution VGA format. We also modified the TIGA interface board by replacing a higher frequency oscillator with a slower 28 MHZ oscillator. The VisionWorks software allowed for complete control over image parameters to include spatial and temporal frequencies, size of grating patch, screen position, spatial frequency orientation, grating contrast, and either counterphase or drifting grating presentation. The video output signal was calibrated and was found to be relatively flat across all spatial frequencies.

The Pritchard 1980A photometer* had a horizontal slit aperture length of only about 0.2 degrees. The photometer was focused to infinity so that the grating pattern was focused sharply. In front of the photometer's objective lens, we placed a 7-mm iris which eliminated the deleterious effect of spherical aberration. Our intention was to use an iris which approximated the pupil size of human observers using the HDU, which would be on the order of 3 or 4 mm

26

given the luminance range of the system. However at this size pupil, insufficient light would have reached the photometer, and this would have affected the temporal response of the photometer at the levels tested. We aligned the slit in the middle of the display (as marked by a test target). As with the temporal measurements, the filtered voltage output from the photometer was fed to a Tektronix 2440 storage oscilloscope* and the Michaelson contrast was computed. The photograph in Figure 20 shows the experimental setup for measuring the MTF.

The nonnormalized spatiotemporal MTF of the system is shown in Figure 21. Each curve represents a different temporal frequency. As expected, there was a strong trend for decreasing contrast with increasing spatial frequency. Although the spatial frequencies seem low, our highest spatial frequency was 4.0 c/deg which corresponds to 120 cycles per vertical display height. We found that low temporal frequency curves overlapped well, but the curves at 4 Hz and 8 Hz showed a significant increase in contrast (approximately 10 percent and 15 percent increase, respectively). This rise in contrast at the high temporal frequencies was not expected since we saw no significant rise in the temporal response curves (Figure 19). We have no reasonable explanation for this high temporal frequency effect.
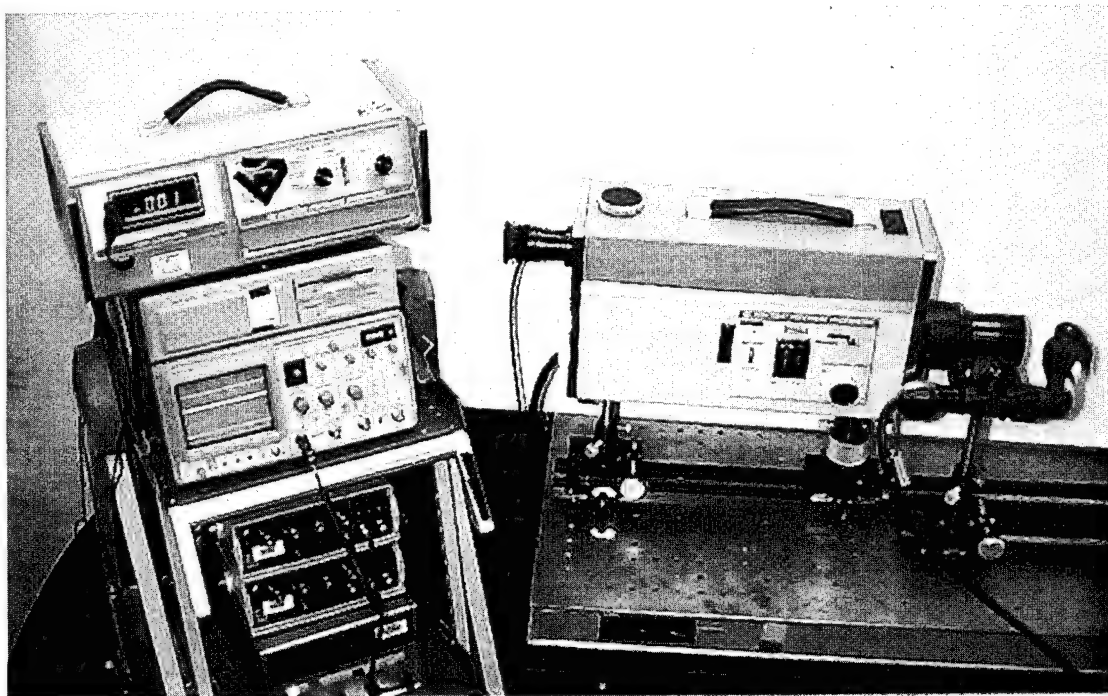
Figure 20. Photograph of test setup for measuring the spatiotemporal MTF.
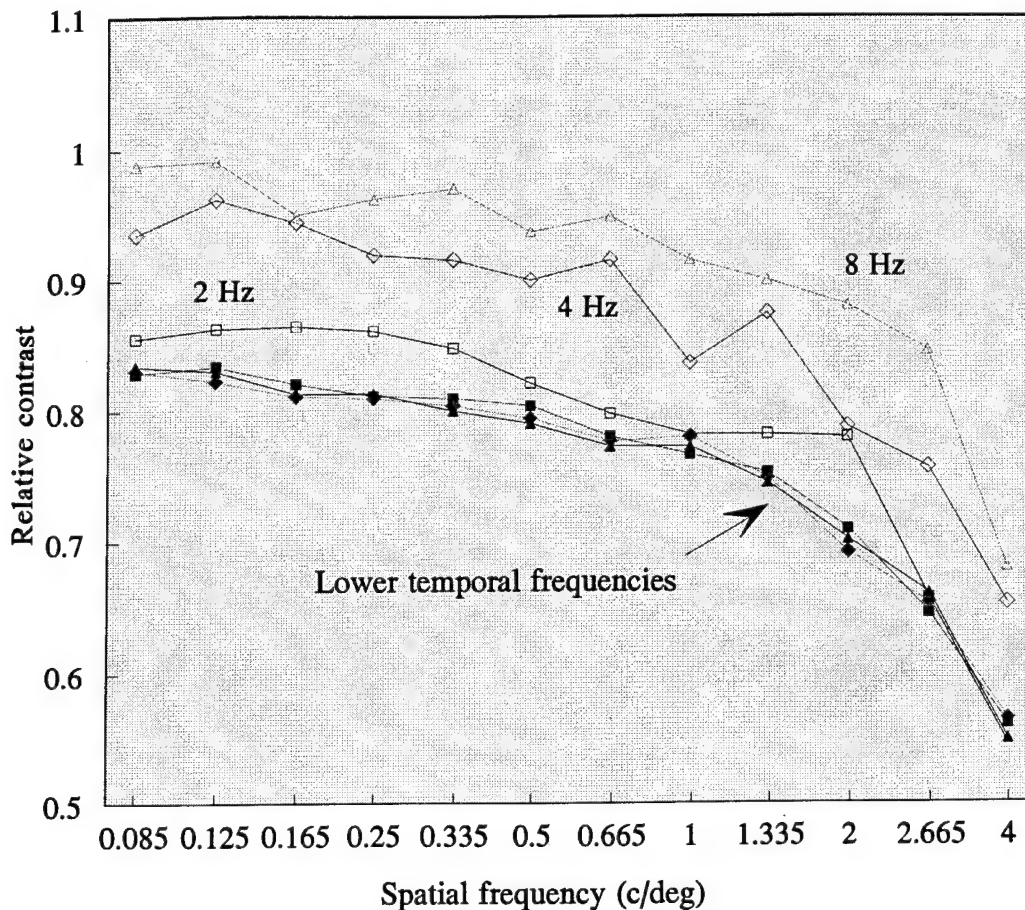
Figure 21. Spatiotemporal MTF of the IHADSS HDU.

Discussion

The IHADSS has been successfully fielded for a decade now, and its performance forms a basis for comparing all future HMD systems. To better understand the performance characteristics of the IHADSS HDU, we undertook this project to quantify important physical characteristics and performance figures-of-merit. We examined the optical characteristics of the HDU to include physical and optical eye relief, exit pupil characteristics, light transmittance and reflectance, optical aberrations, and field-of-view. We also examined the performance characteristics of the IHADSS imagery to include luminance range and available gray shades, spectral output of IHADSS imagery, and spatial and temporal response characteristics.

The exit pupil formed by the HDU was found to be about 10.5 mm in diameter and positioned approximately 57 mm behind the HDU's objective lens. The 57-mm optical path length provided an optical eye relief of about 40 mm with the combiner lens retracted and

28

about 26 mm with the combiner lens fully extended. Of more importance, physical eye relief also was measured for the two combiner lens positions. With the combiner lens retracted, physical eye relief measured about 13 mm. With the combiner lens fully extended, however, we found a <u>negative</u> physical eye relief of about 6-mm.

The field-of-view of the HDU measured approximately 40 degrees by 31 degrees by interpreting the luminance curves shown in Figure 9. The luminance output of the HDU was quite high (luminance saturation equaled about 600 fL). Setting the maximum to 15 and 150 fL, we found contrast ratios of 13.6 and 33.3 which provided a respectable 8 and 11 gray shades, respectively.

The spectral output of the HDU was narrow banded and peaked at 544 nm, corresponding to the peak of the P-43 phosphor. The combiner lens forms an approximate 38 degree angle to the barrel of the HDU. At 38 degrees, the spectral reflectance is banded and peaks at 550 nm. At this angle, about 90 percent of the light emitted from the HDU is reflected into the eye. The combiner forms an angle which is about 23 degrees off normal to the visual line of sight. At this angle, the transmittance is relatively low, and at 544 nm only about 10 percent of the light is transmitted to the eye.

Optically, the IHADSS is a relatively good system. Spherical aberration was certainly low and of little consequence. However, our measurement of field curvature showed a full diopter increase in the periphery with quite noticeable astigmatic aberration. The astigmatic axis was located at about 105 degrees.

The temporal response of the HDU was superb. The temporal response function was flat out to 16 Hz which was the highest frequency tested. The spatiotemporal MTF likewise showed a superb temporal response. Spatially, we saw the anticipated reduction in contrast with increases in spatial frequency. At 4 cycles/deg, contrast was down to about 70 percent of maximum. Since the symbology displayed on the HDU generally is comprised of low spatial frequencies, this fall-off of contrast does not seem to be of significant consequence.

<u>Reference</u>

Hughes Helicopters, Inc. 1982. Procurement specification for the production Integrated Helmet and Display Sight System (IHADSS). PS-14-11077D, 16 March 1982.

APPENDIX

List of manufacturers.

Ann Arbor Optical Co.
Ann Arbor, MI

Gamma Scientific, Inc.
3777 Ruffin Road
San Diego, CA 92123

Honeywell Inc.
1625 Zarthan Ave
St. Louis Park, MN 55416

Hughes Helicopters, Inc
P.O. Box 902
El Segundo, CA   90245-0902

Photo Research, Inc.
9330 Desoto Ave., PO Box 2192
Chatsworth, CA 91313-2192

Tektronix, Inc.
26600 SW Parkway, PO Box 1000
Wilsonville, OR 97070-1000

Texas Instruments
P.O. Box 52
Lubbock, TX 79408

Vision Research Graphics
99 Madbury Road
Durham, NH 03824

Initial distribution

Commander, U.S. Army Natick Research,
    Development and Engineering Center
ATTN: SATNC-MIL (Documents
    Librarian)
Natick, MA 01760-5040

Chairman
National Transportation Safety Board
800 Independence Avenue, S.W.
Washington, DC 20594

Commander
10th Medical Laboratory
ATTN: Audiologist
APO New York 09180

Naval Air Development Center
Technical Information Division
Technical Support Detachment
Warminster, PA 18974

Commanding Officer, Naval Medical
    Research and Development Command
National Naval Medical Center
Bethesda, MD 20814-5044

Deputy Director, Defense Research
    and Engineering
ATTN: Military Assistant
    for Medical and Life Sciences
Washington, DC 20301-3080

Commander, U.S. Army Research
    Institute of Environmental Medicine
Natick, MA 01760

Library
Naval Submarine Medical Research Lab
Box 900, Naval Sub Base
Groton, CT 06349-5900

Executive Director, U.S. Army Human
    Research and Engineering Directorate
ATTN: Technical Library
Aberdeen Proving Ground, MD 21005

Commander
Man-Machine Integration System
Code 602
Naval Air Development Center
Warminster, PA 18974

Commander
Naval Air Development Center
ATTN: Code 602-B
Warminster, PA 18974

Commanding Officer
Armstrong Laboratory
Wright-Patterson
Air Force Base, OH 45433-6573

Director
Army Audiology and Speech Center
Walter Reed Army Medical Center
Washington, DC 20307-5001

Commander/Director
U.S. Army Combat Surveillance
    and Target Acquisition Lab
ATTN: SFAE-IEW-JS
Fort Monmouth, NJ 07703-5305

Director
Federal Aviation Administration
FAA Technical Center
Atlantic City, NJ 08405

Director
Walter Reed Army Institute of Research
Washington, DC 20307-5100

31

Commander, U.S. Army Test
   and Evaluation Command
Directorate for Test and Evaluation
ATTN: AMSTE-TA-M (Human Factors
   Group)
Aberdeen Proving Ground,
   MD 21005-5055

Naval Air Systems Command
Technical Air Library 950D
Room 278, Jefferson Plaza II
Department of the Navy
Washington, DC 20361

Director
U.S. Army Ballistic
   Research Laboratory
ATTN: DRXBR-OD-ST Tech Reports
Aberdeen Proving Ground, MD 21005

Commander
U.S. Army Medical Research
   Institute of Chemical Defense
ATTN: SGRD-UV-AO
Aberdeen Proving Ground,
MD 21010-5425

Commander
USAMRMC
ATTN: SGRD-RMS
Fort Detrick, Frederick, MD 21702-5012

HQ DA (DASG-PSP-O)
5109 Leesburg Pike
Falls Church, VA 22041-3258

Harry Diamond Laboratories
ATTN: Technical Information Branch
2800 Powder Mill Road
Adelphi, MD 20783-1197

Headquarters (ATMD)
U.S. Army Training

and Doctrine Command
ATTN: ATBO-M
Fort Monroe, VA 23651

U.S. Army Materiel Systems
   Analysis Agency
ATTN: AMXSY-PA (Reports Processing)
Aberdeen Proving Ground
MD 21005-5071

U.S. Army Environmental
   Hygiene Agency
ATTN: HSHB-MO-A
Aberdeen Proving Ground, MD 21010

Technical Library Chemical Research
   and Development Center
Aberdeen Proving Ground, MD
21010-5423

Commander
U.S. Army Medical Research
   Institute of Infectious Disease
ATTN: SGRD-UIZ-C
Fort Detrick, Frederick, MD 21702

Director, Biological
   Sciences Division
Office of Naval Research
600 North Quincy Street
Arlington, VA 22217

Commandant
U.S. Army Aviation
   Logistics School ATTN: ATSQ-TDN
Fort Eustis, VA 23604

Eduardo Mera, M.D.
P. O. Box 86715
Bogota, Columbia

Naval Aerospace Medical
Institute Library
Building 1953, Code 03L
Pensacola, FL 32508-5600

Command Surgeon
HQ USCENTCOM (CCSG)
U.S. Central Command
MacDill Air Force Base, FL 33608

Director
Directorate of Combat Developments
ATTN: ATZQ-CD
Building 515
Fort Rucker, AL 36362

U.S. Air Force Institute
of Technology (AFIT/LDEE)
Building 640, Area B
Wright-Patterson
Air Force Base, OH 45433

Henry L. Taylor
Director, Institute of Aviation
University of Illinois-Willard Airport
Savoy, IL 61874

Chief, National Guard Bureau
ATTN: NGB-ARS
Arlington Hall Station
111 South George Mason Drive
Arlington, VA 22204-1382

AAMRL/HEX
Wright-Patterson
Air Force Base, OH 45433

Commander
U.S. Army Aviation and Troop Command
ATTN: AMSAT-R-ES
4300 Goodfellow Bouvelard
St. Louis, MO 63120-1798

U.S. Army Aviation and Troop Command
Library and Information Center Branch
ATTN: AMSAV-DIL
4300 Goodfellow Boulevard
St. Louis, MO 63120

Federal Aviation Administration
Civil Aeromedical Institute
Library AAM-400A
P.O. Box 25082
Oklahoma City, OK 73125

Commander
U.S. Army Medical Department
and School
ATTN: Library
Fort Sam Houston, TX 78234

Commander
U.S. Army Institute of Surgical Research
ATTN: SGRD-USM
Fort Sam Houston, TX 78234-6200

Air University Library
(AUL/LSE)
Maxwell Air Force Base, AL 36112

Product Manager
Aviation Life Support Equipment
ATTN: SFAE-AV-LSE
4300 Goodfellow Boulevard
St. Louis, MO 63120-1798

Commander and Director
USAE Waterways Experiment Station
ATTN: CEWES-IM-MI-R,
CD Department
3909 Halls Ferry Road
Vicksburg, MS 39180-6199

Commanding Officer
Naval Biodynamics Laboratory
P.O. Box 24907
New Orleans, LA 70189-0407

Assistant Commandant
U.S. Army Field Artillery School
ATTN: Morris Swott Technical Library
Fort Sill, OK 73503-0312

Mr. Peter Seib
Human Engineering Crew Station
Box 266
Westland Helicopters Limited
Yeovil, Somerset BA20 2YB UK

U.S. Army Dugway Proving Ground
Technical Library, Building 5330
Dugway, UT 84022

U.S. Army Yuma Proving Ground
Technical Library
Yuma, AZ 85364

AFFTC Technical Library
6510 TW/TSTL
Edwards Air Force Base,
CA 93523-5000

Commander
Code 3431
Naval Weapons Center
China Lake, CA 93555

Aeromechanics Laboratory
U.S. Army Research and Technical Labs
Ames Research Center, M/S 215-1
Moffett Field, CA 94035

Sixth U.S. Army
ATTN: SMA
Presidio of San Francisco, CA 94129

Commander
U.S. Army Aeromedical Center
Fort Rucker, AL 36362

Strughold Aeromedical Library
Document Service Section
2511 Kennedy Circle
Brooks Air Force Base, TX 78235-5122

Dr. Diane Damos
Department of Human Factors
ISSM, USC
Los Angeles, CA 90089-0021

U.S. Army White Sands
   Missile Range
ATTN: STEWS-IM-ST
White Sands Missile Range, NM 88002

Director, Airworthiness Qualification Test
Directorate (ATTC)
ATTN: STEAT-AQ-O-TR (Tech Lib)
75 North Flightline Road
Edwards Air Force Base, CA 93523-6100

Ms. Sandra G. Hart
Ames Research Center
MS 262-3
Moffett Field, CA 94035

Commander
USAMRMC
ATTN: SGRD-UMZ
Fort Detrick, Frederick, MD 21702-5009

Commander
U.S. Army Health Services Command
ATTN: HSOP-SO
Fort Sam Houston, TX 78234-6000

U. S. Army Research Institute
Aviation R&D Activity
ATTN: PERI-IR
Fort Rucker, AL 36362

Commander
U.S. Army Safety Center
Fort Rucker, AL 36362

U.S. Army Aircraft Development
  Test Activity
ATTN: STEBG-MP-P
Cairns Army Air Field
Fort Rucker, AL 36362

Commander
USAMRMC
ATTN: SGRD-PLC (COL R. Gifford)
Fort Detrick, Frederick, MD 21702

TRADOC Aviation LO
Unit 21551, Box A-209-A
APO AE 09777

Netherlands Army Liaison Office
Building 602
Fort Rucker, AL 36362

British Army Liaison Office
Building 602
Fort Rucker, AL 36362

Italian Army Liaison Office
Building 602
Fort Rucker, AL 36362

Directorate of Training Development
Building 502
Fort Rucker, AL 36362

Chief
USAHEL/USAAVNC Field Office
P. O. Box 716
Fort Rucker, AL 36362-5349

Commander, U.S. Army Aviation Center
  and Fort Rucker
ATTN: ATZQ-CG
Fort Rucker, AL 36362

Dr. Sehchang Hah
Dept. of Behavior Sciences and
  Leadership, Building 601, Room 281
U. S. Military Academy
West Point, NY 10996-1784

Canadian Army Liaison Office
Building 602
Fort Rucker, AL 36362

German Army Liaison Office
Building 602
Fort Rucker, AL 36362

French Army Liaison Office
USAAVNC (Building 602)
Fort Rucker, AL 36362-5021

Australian Army Liaison Office
Building 602
Fort Rucker, AL 36362

Dr. Garrison Rapmund
6 Burning Tree Court
Bethesda, MD 20817

Commandant, Royal Air Force
Institute of Aviation Medicine
Farnborough, Hampshire GU14 6SZ UK

Defense Technical Information
Cameron Station, Building 5
Alexandra, VA 22304-6145

Commander, U.S. Army Foreign Science
  and Technology Center
AIFRTA (Davis)
220 7th Street, NE
Charlottesville, VA 22901-5396

Commander
Applied Technology Laboratory
USARTL-ATCOM
ATTN: Library, Building 401
Fort Eustis, VA 23604

Commander, U.S. Air Force
  Development Test Center
101 West D Avenue, Suite 117
Eglin Air Force Base, FL 32542-5495

Aviation Medicine Clinic
TMC #22, SAAF
Fort Bragg, NC 28305

Dr. H. Dix Christensen
Bio-Medical Science Building, Room 753
Post Office Box 26901
Oklahoma City, OK 73190

Commander, U.S. Army Missile
  Command
Redstone Scientific Information Center
ATTN: AMSMI-RD-CS-
      R/ILL Documents
Redstone Arsenal, AL 35898

Aerospace Medicine Team
HQ ACC/SGST3
162 Dodd Boulevard, Suite 100
Langley Air Force Base,
VA 23665-1995

Commander
USAMRMC
ATTN: SGRD-ZC (COL John F. Glenn)
Fort Detrick, Frederick, MD 21702-5012

U.S. Army Research and Technology
  Laboratories (AVSCOM)
Propulsion Laboratory MS 302-2
NASA Lewis Research Center
Cleveland, OH 44135

Dr. Eugene S. Channing
166 Baughman's Lane
Frederick, MD 21702-4083

U.S. Army Medical Department
  and School
USAMRDALC Liaison
ATTN: HSMC-FR
Fort Sam Houston, TX 78234

NVESD
AMSEL-RD-NV-ASID-PST
(Attn: Trang Bui)
10221 Burbeck Road
Fort Belvior, VA 22060-5806

CA Av Med
HQ DAAC
Middle Wallop
Stockbridge, Hants S020 8DY UK

Dr. Christine Schlichting
Behavioral Sciences Department
Box 900, NAVUBASE NLON
Groton, CT 06349-5900

Commander
Aviation Applied Technology Directorate
ATTN: AMSAT-R-TV
Fort Eustis, VA 23604-5577

COL Yehezkel G. Caine, MD
Surgeon General, Israel Air Force
Aeromedical Center Library
P. O. Box 02166 I.D.F.
Israel

HQ ACC/DOHP
205 Dodd Boulevard, Suite 101
Langley Air Force Base,
VA 23665-2789

41st Rescue Squadron
41st RQS/SG
940 Range Road
Patrick Air Force Base,
FL 32925-5001

48th Rescue Squadron
48th RQS/SG
801 Dezonia Road
Holloman Air Force Base,
NM 88330-7715

HQ, AFOMA
ATTN: SGPA (Aerospace Medicine)
Bolling Air Force Base,
Washington, DC 20332-6128

ARNG Readiness Center
ATTN: NGB-AVN-OP
Arlington Hall Station
111 South George Mason Drive
Arlington, VA 22204-1382

35th Fighter Wing
35th FW/SG
PSC 1013
APO AE 09725-2055

66th Rescue Squadron
66th RQS/SG
4345 Tyndall Avenue
Nellis Air Force Base, NV 89191-6076

71st Rescue Squadron
71st RQS/SG
1139 Redstone Road
Patrick Air Force Base,
FL 32925-5000

Director
Aviation Research, Development
  and Engineering Center
ATTN: AMSAT-R-Z
4300 Goodfellow Boulevard
St. Louis, MO 63120-1798

Commander
USAMRMC
ATTN: SGRD-ZB (COL C. Fred Tyner)
Fort Detrick, Frederick, MD 21702-5012

Commandant
U.S. Army Command and General Staff
  College
ATTN: ATZL-SWS-L
Fort Levenworth, KS 66027-6900

Director
Army Personnel Research Establishment
Farnborough, Hants GU14 6SZ UK

Dr. A. Kornfield
895 Head Street
San Francisco, CA 94132-2813

Mr. George T. Singley, III
Depupty Assistant Secretary of the Army
  for Research and Technology
  and Chief Scientist
ATTN: Room 3E374
103 Army Pentagon
Washington, DC 20310-0103

The Honorable Gilbert F. Decker
Assistant Secretary of the Army
  for Research, Development,
  and Acquisition
ATTN: Room 2E672
103 Army Pentagon
Washington, DC 20310-0103

Dr. Craig Dorman
Office of the Deputy Director,
  Defense Research and Engineering
ATTN: Room 3D129LM
103 Army Pentagon
Washington, DC 20310-0103

HQ, AFOMA
ATTN; SGPA (Aerospace Medicine)
Bolling Air Force Base,
Washington, DC 20332-6188

Cdr, PERSCOM
ATTN: TAPC-PLA
200 Stovall Street, Rm 3N25
Alexandria, VA 22332-0413